Anti-acceleration Saturation Terminal Guidance Law Based on LSTM

LI Guilin, ZHOU Wei, ZHANG Jiaru*

School of Electrical Engineering and Automation, Jiangsu Normal University, Xuzhou 221116, P. R. China

(Received 10 April 2025; revised 30 July 2025; accepted 1 August 2025)

Abstract: Missile acceleration saturation in a practical terminal guidance process may significantly reduce the interception performance. To solve this problem, this paper presents an anti-saturation guidance law with finite-time convergence for a three dimensional maneuvering interception. The finite time boundedness (FTB) theory and the input-output finite time stability (IO-FTS) theory are used, as well as the long short-term memory (LSTM) network. A sufficient condition for FTB and IO-FTS of a class of nonlinear systems is given. Then, an anti-acceleration saturation missile terminal guidance law based on LSTM, namely LSTM-ASGL, is designed. It can effectively suppress the effect of acceleration saturation to track the maneuvering target more accurately in the complex dynamic environment. The excellent performance of LSTM-ASGL in different maneuvering target scenarios is verified by simulation. The simulation results show that the guidance law successfully prevents acceleration saturation and improves the tracking ability of the missile system to the maneuvering target. It is also shown that LSTM-ASGL has good generalization and anti-jamming performance, and consumes less energy than the anti-acceleration saturation terminal guidance law.

Key words: long short-term memory network (LSTM); anti-acceleration saturation; terminal guidance law; finite-time boundedness (FTB); input-output finite time stability (IO-FTS)

CLC number: TJ765 **Document code:** A **Article ID:** 1005-1120(2025)04-0541-13

0 Introduction

With the rapid development of highly intelligent guidance technology, the traditional missile guidance system is facing unprecedented challenges.

In practice, the missile's acceleration may reach its physical limit, which may greatly degrade the missile's interception performance. Acceleration saturation prevents the missile from generating sufficient normal acceleration to track the target's maneuvers, weakening its ability to quickly suppress the line-of-sight rate. This leads to a decline in the closed-loop stability of the guidance system, ultimately increasing the miss distance. The main objective of the anti-acceleration saturation guidance law is to prevent acceleration saturation that may occur in the interception mission. In Ref.[1], a guidance method for three-dimensional (3D) interception of maneuvering targets with anti-saturation capability was proposed. The guidance law was designed based on the principles of finite-time boundedness (FTB) and the input-output finite-time stability (IO-FTS), ensuring convergence of the line-of-sight (LOS) angular rate within a finite time while constraining the missile acceleration within its limit, thereby enhancing interception performance.

In Ref.[2], an improved proportional navigation guidance (PNG) law was proposed to consider error anti-saturation. In Ref.[3], a varying-gain PNG law is proposed, combined with a biased feedback command to obtain an impact time control guidance law. The core drawbacks of the PNG law lie in fundamental limitations such as strong model dependence, insufficient anti-saturation ability, and

*Corresponding author, E-mail address: 2020221773@jsnu.edu.cn.

How to cite this article: LI Guilin, ZHOU Wei, ZHANG Jiaru. Anti-acceleration saturation terminal guidance law based on LSTM[J]. Transactions of Nanjing University of Aeronautics and Astronautics, 2025,42(4):541-553.

http://dx.doi.org/10.16356/j.1005-1120.2025.04.009

the inability of fixed parameters to dynamically adapt to target maneuvers. In Ref.[4], a 3D sliding-mode guidance law was proposed for intercepting maneuvering targets with specified performance and saturated actuators. Based on the two-dimensional relative motion model of the missile and target, Ref.[5] proposed a 3D fixed-time convergence guidance law for intercepting highly maneuvering targets. By employing innovative fixed-timed convergent sliding mode surface design and inverse control methods, the issues of guidance command input saturation and system disturbances were addressed. In Ref.[6], an anti-saturation guidance law based on a finite-time observer was designed. To address the issue of requiring an upper bound of the observation error, a new reaching law was proposed, which can accelerate the convergence rate of sliding mode surfaces and mitigate the chattering phenomenon. In Ref.[7], a time-varying sliding mode guidance law considering the second-order autopilot dynamics and input saturation was proposed. Utilizing the extended state observer, this guidance law does not require information on the target acceleration and interceptor acceleration derivatives. The core limitations of sliding mode guidance lie in the trade-off between chattering and robustness, as well as the inadequate adaptability of fixed structures to time-varying environments. Although these studies have partially mitigated these issues through improved reaching laws, observer introduction, or time-varying sliding surface design, the fundamental challenges of chattering and dynamic adaptability remain unresolved.

The traditional missile terminal guidance laws are usually not adaptive to uncertainties and disturbances with limited real-time performance in different environments and conditions. Therefore, more intelligent guidance laws with strong real-time adaptability and resistance to saturation effects are worth investigating.

In Ref.[8], a deep neural network guidance (DNNG) law was proposed to replace PNG. Its performance was evaluated through the hit ratio and energy function, and a conclusion was drawn that DNNG could completely imitate and replace PNG. In Ref.[9], a deep reinforcement learning (DRL) algorithm was used to design the impact-time control guidance with a time-varying velocity. In Ref.[10], the optimal guidance conditions were derived based on the Pontryagin's maximum principle and transformed into a backward integration problem. A neural network was trained on the dataset to approximate the optimal guidance command, and an optimal terminal guidance scheme combining the neural network with biased proportional navigation was proposed. In Ref.[11], a collaborative guidance strategy for aircraft to evade missiles was proposed by using DRL. The multi-agent game method was adopted, and a general reward function was designed to solve the sparse reward problem. In Ref.[12], an integrated transfer learning guidance algorithm was proposed for angular-constrained midcourse guidance. The algorithm aims to maximize the final speed and improve the learning efficiency through the generalization ability of deep neural networks in new environments. In Ref.[13], a novel guidance law based on reinforcement learning (RL) was proposed, using a twin-delayed deep deterministic policy gradient neural network to solve the maneuvering target interception problem.

Recurrent neural network (RNN) and its variant the long short-term memory (LSTM) network have many advantages in missile terminal guidance. In Ref.[14], the gradient algorithm of the recorded recurrent twin delayed deep deterministic strategy was proposed to address the uncertainty and observation noise in the guidance law of intercepting atmospheric maneuvering targets. RNN is introduced to improve the performance of DRL in partially observable decision processes. In Ref.[15], a time cooperation framework was proposed for the design of multiple hypersonic vehicle guidance systems. The longitudinal prediction correction guidance law was used to satisfy both terminal and path constraints, and LSTM was used to solve the problem of inaccurate estimation of the remaining flight time. During missile flight, the target's motion is complex and time-dependent, and acceleration saturation is also time-related. LSTM, with its gating mechanism, effectively captures long-term sequence information, predicting acceleration saturation based on the

target's historical motion and the missile's acceleration changes, as well as adjusts the guidance strategy in advance. Feedforward neural networks rely only on current inputs and cannot utilize historical information, making them less effective in predicting acceleration saturation. Convolutional neural networks are suited for spatial data and have limited ability to capture long-term dependencies, making them less effective than LSTM. Simple recurrent neural networks can process time series but suffer from gradient vanishing, affecting prediction reliability and making them less reliable than LSTM.

To overcome the limitation of traditional guidance laws and mitigate the effect of acceleration saturation on the performance of missile systems, an anti-acceleration saturation missile terminal guidance law, namely ASGL, based on LSTM is designed in this paper, named as LSTM-ASGL. The existing 3D anti-acceleration saturation guidance law is modeled and simulated by using the LSTM network. The LSTM model is trained with a large number of training data sets obtained from the anti-acceleration saturation guidance law. Simulation experiments show that LSTM-ASGL has the characteristics of anti-acceleration saturation and anti-interference, and for different types of maneuvering targets, LSTM-ASGL can predict the target maneuvers accurately.

1 Anti-acceleration Saturation Terminal Guidance Law Design

1.1 3D missile-target equations of motion

Fig.1 shows the 3D relative motion diagram of the missile and the target.

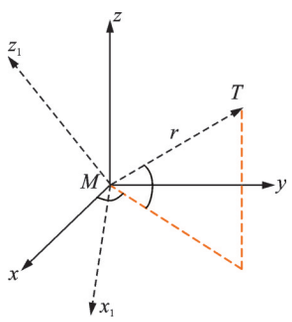

Fig.1 Schematic diagram of a typical radar system

In Fig.1, $Mxyz$ is the reference inertial coordinate system. $Mx_1y_1z_1$ is the line of sight coordinate system. And M and T are the center of mass of the missile and the target, respectively. r is the relative distance between the missile and the target. θ and ϕ are the azimuth and pitch angles, respectively. Assuming that the acceleration components of the missile and the target are $(a_{Mr}, a_{M\theta}, a_{M\phi})$ and $(a_{Tr}, a_{T\theta}, a_{T\phi})$, respectively. The relative motion of the missile and target can be described as

$$\ddot{r} = r\dot{\theta}^2\cos^2\phi + r\dot{\phi}^2 + a_{Tr} - a_{Mr} \tag{1a}$$

$$r\ddot{\theta}\cos\phi = -2\dot{r}\dot{\theta}\cos\phi + 2r\dot{\phi}\dot{\theta}\sin\phi + a_{T\theta} - a_{M\theta} \tag{1b}$$

$$r\ddot{\phi} = -2\dot{r}\dot{\phi} - r\dot{\theta}\sin\phi\cos\phi + a_{T\phi} - a_{M\phi} \tag{1c}$$

Assume that the missile autopilot has the first-order dynamics in both directions of θ and ϕ

$$\dot{a}_{M\theta} = -1/\tau a_{M\theta} + 1/\tau u_1 \tag{2a}$$

$$\dot{a}_{M\phi} = -1/\tau a_{M\phi} + 1/\tau u_2 \tag{2b}$$

where τ is the time constant; and $\boldsymbol{u} = [u_1, u_2]^{\mathrm{T}}$ the controller input to the autopilot.

Since the guidance objective is to eliminate line-of-sight angular rates $\dot{\theta}$ and $\dot{\phi}$, the radial acceleration a_{Mr} will not be considered.

Assumption 1 The missile accelerations satisfy

$$|a_{M\theta}| \leqslant a_{M\theta_{\max}}, \quad |a_{M\phi}| \leqslant a_{M\phi_{\max}} \tag{3}$$

where $a_{M\theta_{\max}} \geqslant 0$ and $a_{M\phi_{\max}} \geqslant 0$ are the given acceleration upper bounds.

The system state vector is defined as $\boldsymbol{x}(t) = [x_1, x_2, x_3, x_4]^{\mathrm{T}} = [\dot{\theta}\cos\phi, \dot{\phi}, a_{M\theta}, a_{M\phi}]^{\mathrm{T}}$, the normal accelerations of the target are considered as disturbance $\boldsymbol{w}(t) = [w_1, w_2]^{\mathrm{T}} = [a_{T\theta}, a_{T\phi}]^{\mathrm{T}}$, and the state equations are obtained as

$$\dot{x}_1 = -2\dot{r}(t)/r(t)x_1 - 1/r(t)x_3 + x_1x_2\tan\phi + 1/r(t)w_1 \tag{4a}$$

$$\dot{x}_2 = -2\dot{r}(t)/r(t)x_2 - 1/r(t)x_4 - x_1^2\tan\phi + 1/r(t)w_2 \tag{4b}$$

$$\dot{x}_3 = -1/\tau x_3 + 1/\tau u_1 \tag{4c}$$

$$\dot{x}_4 = -1/\tau x_4 + 1/\tau u_2 \tag{4d}$$

Remark 1 Eq.(4) is singular when $r = 0$. Since the missile and the target have a certain size, as long as r is reduced to a small enough value, a successful intercept can be achieved. Therefore, $r >$

0 holds during the terminal guidance phase. And $\cos\phi$ holds as long as a reasonable reference inertial coordinate is selected.

The guidance problem is to design the guidance law under the system (4), so that the missile can successfully intercept a maneuvering target in a finite time while ensuring that its acceleration does not exceed its physical limit, that is, to meet the constraint (3).

1.2 Definitions and preliminaries

In this paper, $\boldsymbol{I}_k$ represents a $k\times k$ identity matrix and $\langle\cdot,\cdot\rangle$ the inner product in the Euclidean space.

Consider a linear time-varying system (5)

$$\dot{\boldsymbol{x}}(t)=\boldsymbol{A}(t)\boldsymbol{x}(t)+\boldsymbol{G}(t)\boldsymbol{w}(t) \tag{5a}$$

$$\boldsymbol{y}(t)=\boldsymbol{C}(t)\boldsymbol{x}(t) \tag{5b}$$

where $\boldsymbol{x}(t)\in\mathbf{R}^n$, $\boldsymbol{w}(t)\in\mathbf{R}^r$ and $\boldsymbol{y}(t)\in\mathbf{R}^l$ represent the system state vector, the external disturbance, and the system output, respectively. $\boldsymbol{A}(t)\in\mathbf{R}^{n\times n}$, $\boldsymbol{G}(t)\in\mathbf{R}^{n\times r}$, and $\boldsymbol{C}(t)\in\mathbf{R}^{l\times n}$ are known matrix-valued functions.

Definition 1 (FTB) Given a positive scalar T, a positive definite matrix $\boldsymbol{H}$, and a positive definite matrix-valued function $\boldsymbol{\Gamma}(\cdot)$ which are defined in the finite time interval $[0,T]$, and $\boldsymbol{\Gamma}(0)<\boldsymbol{H}$. $\boldsymbol{w}(t)$ satisfies

$$\int_0^T\boldsymbol{w}^{\mathrm{T}}(t)\boldsymbol{D}_{\mathrm{w}}\boldsymbol{w}(t)\mathrm{d}t\leqslant 1\qquad\forall\boldsymbol{w} \tag{6}$$

where $\boldsymbol{D}_{\mathrm{w}}\in\mathbf{R}^{r\times r}$ is a given positive definite matrix, if the system (5) is satisfied

$$\boldsymbol{x}_0^{\mathrm{T}}\boldsymbol{H}\boldsymbol{x}_0\leqslant 1\Rightarrow\boldsymbol{x}^{\mathrm{T}}(t)\boldsymbol{\Gamma}(t)\boldsymbol{x}(t)<1\qquad\forall t\in[0,T] \tag{7}$$

The system (5) is said to be finite time bounded with respect to $(T,\boldsymbol{H},\boldsymbol{\Gamma}(\cdot),\boldsymbol{D}_{\mathrm{w}})$.

Definition 2 (IO-FTS) Consider the system (5) with $x_0=0$. If the system (5) satisfies

$$\int_0^T\boldsymbol{w}^{\mathrm{T}}(t)\boldsymbol{D}_{\mathrm{w}}\boldsymbol{w}(t)\mathrm{d}t\leqslant 1\Rightarrow\boldsymbol{y}^{\mathrm{T}}(t)\boldsymbol{N}(t)\boldsymbol{y}(t)\leqslant 1\qquad\forall t\in[0,T] \tag{8}$$

where $\boldsymbol{N}(\cdot)$ is a positive definite matrix-valued function. The system (5) is said to be input-output finite-time stable with respect to $(T,\boldsymbol{H},\boldsymbol{\Gamma}(\cdot))$.

Since both the initial conditions and the inputs affect the state and output of the system, Definition 2 is given under zero initial conditions. However, for a linear system, the effect can be superimposed, and the controller effect is similar whether the controller is designed under zero initial conditions or non-zero initial conditions.

Consider a class of systems

$$\dot{\boldsymbol{x}}(t)=\boldsymbol{A}\boldsymbol{x}(t)+\boldsymbol{B}\boldsymbol{u}(t)+\boldsymbol{\Phi}(\boldsymbol{x},\boldsymbol{u}) \tag{9}$$

where $\boldsymbol{x}(t)\in\mathbf{R}^n$, $\boldsymbol{u}(t)\in\mathbf{R}^m$ are the state and the input of the system, respectively. $\boldsymbol{A}\in\mathbf{R}^{n\times n}$, $\boldsymbol{B}\in\mathbf{R}^{n\times m}$ are constant matrices; and $\boldsymbol{\Phi}(\boldsymbol{x},\boldsymbol{u})$ is a nonlinear function of $\boldsymbol{x}$.

Definition 3 A nonlinear function $\boldsymbol{\Phi}(\boldsymbol{x},\boldsymbol{u})$ is called a quasi-one-sided nonlinear Lipschitz function with a quasi-one-sided Lipschitz constant matrix $\boldsymbol{M}$. If for any $\boldsymbol{x}$, $\hat{\boldsymbol{x}}\in\mathbf{R}^n$, $\boldsymbol{u}\in\mathbf{R}^m$, we have

$$\langle\boldsymbol{P}\boldsymbol{\Phi}(\boldsymbol{x},\boldsymbol{u})-\boldsymbol{P}\boldsymbol{\Phi}(\hat{\boldsymbol{x}},\boldsymbol{u}),\boldsymbol{x}-\hat{\boldsymbol{x}}\rangle\leqslant(\boldsymbol{x}-\hat{\boldsymbol{x}})^{\mathrm{T}}\cdot\boldsymbol{M}(\boldsymbol{x}-\hat{\boldsymbol{x}}) \tag{10}$$

where $\boldsymbol{P}$ is a positive definite matrix to be determined and $\boldsymbol{M}$ a given real symmetric matrix. System (9) is called a quasi-one-sided Lipschitz nonlinear system.

Consider a quasi-one-sided Lipschitz nonlinear system(11)

$$\dot{\boldsymbol{x}}(t)=\boldsymbol{A}(t)\boldsymbol{x}(t)+\boldsymbol{B}(t)\boldsymbol{u}(t)+\boldsymbol{G}(t)\boldsymbol{w}(t)+\boldsymbol{\Phi}(\boldsymbol{x},\boldsymbol{u}) \tag{11a}$$

$$\boldsymbol{y}(t)=\boldsymbol{C}(t)\boldsymbol{x}(t) \tag{11b}$$

where $\boldsymbol{B}(t)\in\mathbf{R}^{n\times m}$ is a known matrix-valued function; $\boldsymbol{\Phi}(0,\boldsymbol{u})=0$; $\boldsymbol{w}(t)$ satisfies the inequality in Eq.(6). According to Definitions 1 and 2, FTB and IO-FTS is defined.

Definition 4 (FTB and IO-FTS) For system (11), the closed-loop system is defined as

$$\dot{\boldsymbol{x}}(t)=\bar{\boldsymbol{A}}(t)\boldsymbol{x}(t)+\boldsymbol{G}(t)\boldsymbol{w}(t)+\boldsymbol{\Phi}(x,u) \tag{12}$$

with a state feedback control law

$$\boldsymbol{u}(t)=\boldsymbol{K}(t)\boldsymbol{x}(t) \tag{13}$$

where $\bar{\boldsymbol{A}}(t)=\boldsymbol{A}(t)+\boldsymbol{B}(t)\boldsymbol{K}(t)$ and $\boldsymbol{K}(t)$ is the control gain to be determined. Eqs.(12,13) satisfy FTB about $(T,\boldsymbol{H},\boldsymbol{\Gamma}(\cdot),\boldsymbol{D}_{\mathrm{w}})$ and IO-FTS about $(T,\boldsymbol{D}_{\mathrm{w}},\boldsymbol{N}(\cdot))$, if the unknown disturbance satisfies the inequality in Eq.(6), and the conditions (7) and (8) hold simultaneously.

Quasi-one-sided Lipschitz condition is employed to address the nonlinear term, and trans-

forms the problem of ensuring the system FTB and IO-FTS simultaneously to that of solving a differential linear matrix inequality (DLMI). To design the state feedback controller of the system (11) using the DLMI technology, we assume that $\boldsymbol{M}$ is positive semidefinite, and then there is a matrix $\boldsymbol{D}\in\mathbf{R}^{n\times n}$ that satisfies

$$\begin{bmatrix} \boldsymbol{K}^{\mathrm{T}}(t)\boldsymbol{B}^{\mathrm{T}}(t)\boldsymbol{P}(t)+\boldsymbol{A}^{\mathrm{T}}(t)\boldsymbol{P}(t)+\dot{\boldsymbol{P}}(t)+\boldsymbol{P}(t)\boldsymbol{A}(t)+\boldsymbol{P}(t)\boldsymbol{B}(t)\boldsymbol{K}(t) & \boldsymbol{P}(t)\boldsymbol{G}(t) & \boldsymbol{D}^{\mathrm{T}} \\ \boldsymbol{G}^{\mathrm{T}}(t)\boldsymbol{P}(t) & -\boldsymbol{D}_{\mathrm{w}} & 0 \\ \boldsymbol{D} & 0 & -1/2\boldsymbol{I}_n \end{bmatrix}<0 \quad (15)$$

$$\boldsymbol{P}(t)\geqslant\max(2\boldsymbol{\Gamma}(t),\boldsymbol{C}^{\mathrm{T}}(t)\boldsymbol{N}(t)\boldsymbol{C}(t)) \quad (16)$$

$$\boldsymbol{P}(0)<\boldsymbol{H} \quad (17)$$

The control gain $\boldsymbol{K}(t)$ of the controller (13) is designed under the three conditions in Theorem 1.

Corollary 1 For quasi-one-sided Lipschitz nonlinear system (11), if there is a positive matrix value function $\boldsymbol{Q}(t)\in\mathbf{R}^{n\times n}$ and a matrix value function $\boldsymbol{E}(t)\in\mathbf{R}^{m\times n}$, and the following three inequalities hold.

$$\begin{bmatrix} \boldsymbol{\Theta}(t) & \boldsymbol{G}(t) & \boldsymbol{Q}\boldsymbol{D}^{\mathrm{T}} \\ \boldsymbol{G}^{\mathrm{T}}(t) & -\boldsymbol{D}_{\mathrm{w}} & 0 \\ \boldsymbol{D}\boldsymbol{Q} & 0 & -1/2\boldsymbol{I}_n \end{bmatrix}<0 \quad (18)$$

$$\boldsymbol{Q}^{-1}(t)\geqslant\max(2\boldsymbol{\Gamma}(t),\boldsymbol{C}^{\mathrm{T}}(t)\boldsymbol{N}\boldsymbol{C}(t)) \quad (19)$$

$$\boldsymbol{Q}^{-1}(0)<\boldsymbol{H} \quad (20)$$

where $\boldsymbol{\Theta}(t)=\boldsymbol{E}^{\mathrm{T}}(t)\boldsymbol{B}^{\mathrm{T}}(t)+\boldsymbol{Q}(t)\boldsymbol{A}^{\mathrm{T}}(t)-\dot{\boldsymbol{Q}}(t)+\boldsymbol{A}(t)\boldsymbol{Q}(t)+\boldsymbol{B}(t)\boldsymbol{E}(t)$. The state feedback control law $\boldsymbol{K}(t)=\boldsymbol{E}(t)\boldsymbol{Q}^{-1}(t)$ makes system (11) satisfy FTB and IO-FTS.

Proof Details can be found in Ref.[1].

1.3 Anti-acceleration saturation guidance law design

Rewrite the state Eq.(4) as

$$\dot{\boldsymbol{x}}(t)=\boldsymbol{A}(t)\boldsymbol{x}(t)+\boldsymbol{B}(t)\boldsymbol{u}(t)+\boldsymbol{G}(t)\boldsymbol{w}(t)+\boldsymbol{\Phi}(x,u) \quad (21)$$

where $\boldsymbol{A}(t)=\begin{bmatrix} -2\dot{r}/r & 0 & -1/r & 0 \\ 0 & -2\dot{r}/r & 0 & -1/r \\ 0 & 0 & -1/\tau & 0 \\ 0 & 0 & 0 & -1/\tau \end{bmatrix}$,

$\boldsymbol{B}(t)=\begin{bmatrix} 0 & 0 \\ 0 & 0 \\ 1/\tau & 0 \\ 0 & 1/\tau \end{bmatrix}$, $\boldsymbol{G}(t)=\begin{bmatrix} 1/r & 0 \\ 0 & 1/r \\ 0 & 0 \\ 0 & 0 \end{bmatrix}$,

$$\boldsymbol{M}=\boldsymbol{D}^{\mathrm{T}}\boldsymbol{D} \quad (14)$$

Theorem 1 Consider a closed loop system (12) with a state feedback controller (13). System (13) satisfies FTB and IO-FTS. If there exists a positive definite matrix-valued function $\boldsymbol{P}(t)\in\mathbf{R}^{n\times n}$, and for any unknown disturbance satisfying Eq.(6), the following three conditions are satisfied

and $\boldsymbol{\Phi}(x,u)=[x_1x_2\tan\phi,\ -x_1^2\tan\phi,\ 0,\ 0]^{\mathrm{T}}$.

Take the output as

$$\boldsymbol{y}(t)=\boldsymbol{C}(t)\boldsymbol{x}(t) \quad (22)$$

where $\boldsymbol{y}(t)=[y_1,y_2]$, $\boldsymbol{C}(t)=\begin{bmatrix} 1 & 0 & 0 & 0 \\ 0 & 1 & 0 & 0 \end{bmatrix}$, and the finite time interval as $[0,t_{\mathrm{f}}]$.

The guidance law $\boldsymbol{u}$ is designed to make systems (21, 22) satisfy FTB and IO-FTS, LOS rates of $\dot{\theta}$ and $\dot{\phi}$ to converge to zero, and the missile acceleration $a_{M\theta}$ and $a_{M\phi}$ to meet the constraint (3).

To use Corollary 1, one needs to verify that the nonlinear function $\boldsymbol{\Phi}(\boldsymbol{x},\boldsymbol{u})$ satisfies Eq.(10). Obviously, $\boldsymbol{\Phi}(0,\boldsymbol{u})=0$.

Apply Eq.(10) with $\hat{\boldsymbol{x}}=0$, then

$$\langle\boldsymbol{P}(t)\boldsymbol{\Phi}(\boldsymbol{x},\boldsymbol{u}),\boldsymbol{x}\rangle\leqslant\boldsymbol{x}^{\mathrm{T}}(t)\boldsymbol{D}^{\mathrm{T}}\boldsymbol{D}\boldsymbol{x}(t) \quad (23)$$

Let a positive definite matrix $\boldsymbol{P}(t)=p\boldsymbol{I}_4$, where p is a positive constant.

Since $\boldsymbol{P}(t)\boldsymbol{\Phi}(\boldsymbol{x},\boldsymbol{u})=[px_1x_2\tan\phi,\ -px_1^2\tan\phi,\ 0,\ 0]^{\mathrm{T}}$

$$\langle\boldsymbol{P}(t)\boldsymbol{\Phi}(\boldsymbol{x},\boldsymbol{u}),\boldsymbol{x}\rangle=\boldsymbol{x}^{\mathrm{T}}\boldsymbol{P}(t)\boldsymbol{\Phi}(\boldsymbol{x},\boldsymbol{u})=0 \quad (24)$$

Following Eq.(14) and the semidefinite properties, the right-hand side of Eq.(23) satisfies

$$\boldsymbol{x}^{\mathrm{T}}\boldsymbol{M}\boldsymbol{x}\geqslant0 \quad (25)$$

For any $\boldsymbol{x}\in\mathbf{R}^4,\boldsymbol{x}\neq0$, the condition (23) holds.

Corollary 2 Consider the terminal guidance systems (21, 22). If there are positive definite matrix-valued functions $\boldsymbol{Q}'(t)\in\mathbf{R}^{4\times4}$ and matrix-valued functions $\boldsymbol{E}'(t)\in\mathbf{R}^{2\times4}$, the matrix inequalities (18—20) hold, and the closed-loop systems (21, 22) have the state feedback guidance law

$$\boldsymbol{u}(t)=\boldsymbol{K}'(t)\boldsymbol{x}(t)\quad\forall t\in[0,T] \quad (26)$$

where $\boldsymbol{K}'(t)=\boldsymbol{E}'(t)\boldsymbol{x}(t)$, the closed-loop system

is FTB-IO-FTS.

Corollary 2 is a direct result of Corollary 1. When tracking a maneuvering target, the guidance law (26) can drive LOS rates $\dot{\theta}$ and $\dot{\phi}$ to converge in a finite time and ensure that the accelerations $a_{M\theta}$ and $a_{M\phi}$ do not exceed the given physical limits in Eq.(3).

The missile actuator or propeller, as well as the maneuverability, is usually limited, which makes it difficult to intercept highly maneuverable targets. If the command acceleration is much greater than the acceptable range that the missile can provide, it will saturate the actuator, which in turn affects the guidance performance. Therefore, to overcome the limitation of missile maneuverability and improve its interception efficiency in intercepting highly maneuverable targets, research on anti-acceleration saturation terminal guidance is particularly important.

2 LSTM Neural Network Design

To further improve the anti-acceleration saturation capability of missile guidance, this paper combines the missile guidance technology with the deep learning technology and uses the LSTM network to control the guidance process. During the missile's flight, the target's motion is complex, and the acceleration saturation is related to time. Thanks to its gating mechanism, LSTM can effectively capture information from long time series. It can accurately predict the acceleration saturation based on the historical motion states of the target and the missile, and then adjust the guidance strategy accordingly.

In contrast, feedforward neural networks do not have memory units and only rely on the current input. As a result, they are unable to make use of historical information and have a weak ability to predict acceleration saturation. Convolutional neural networks are suitable for processing spatial data, but their ability to capture long-term temporal dependencies is limited. Although simple recurrent neural networks can handle time series, they are prone to problems such as gradient vanishing or explosion, resulting in unstable learning and memory capabilities, and their reliability is not as good as that of LSTM.

2.1 Data collection and preprocessing

In this paper, MATLAB is used to simulate the anti-acceleration saturation guidance law, and generate the data set. The data set has line-of-sight angular rates θ and ϕ and time t as inputs, and acceleration components $a_{M\theta}$ and $a_{M\phi}$ as outputs. In the data set, 70% data are randomly selected as the training set, and the rest is used as the test set.

The data sets are normalized to make the numerical ranges of different features similar, and help to improve stability of the model and accelerate the convergence of the model. Different features in the data set may have different scales, which may result in some features having a greater impact on the model. Through normalization, it can avoid the excessive impact of numerical differences on the model, and ensure that the impact of each feature on the model is relatively balanced.

2.2 LSTM model construction

The LSTM model structure is shown in Fig.2.

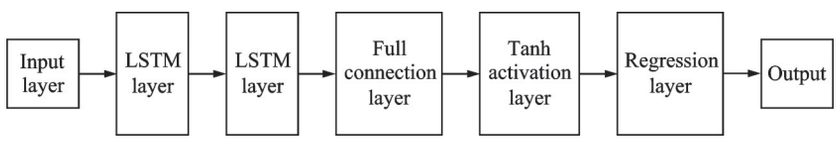

Fig.2 LSTM model structure

The overall architecture of the model includes a sequence of input layer, two LSTM layers, a full connection layer, a Tanh activation layer, and a regression layer. Each LSTM layer has a different number of hidden units and outputs the hidden state of the entire sequence by adjusting the output mode.

The input layer is used to accept the input for the entire sequence. The LSTM layer processes sequential data, captures time sequence information, and can process and remember long-term dependen-

cies in sequence more effectively through the input gate, forgetting gate, output gate, and other mechanisms. The fully connected layer maps the output of the LSTM layer to a fixed-size output space, and by learning weights and biases, the output of the LSTM layer is linearly combined and nonlinear relations are introduced. The Tanh activation layer maps the output of the fully connected layer nonlinearly, helping the network learn more complex patterns. The regression layer calculates the loss between the model output and the guidance law simulation output value, and uses the mean square error loss function to measure the difference between the model output and the actual value to improve the prediction accuracy.

2.3 Data collection and preprocessing

The Adam algorithm is used for optimization of the LSTM model, which combines the advantages of the momentum method and the root mean square propagation (RMSProp) algorithm. By calculating the exponential weighted sum of the moving average gradient and gradient square, the learning rate is dynamically adjusted for each parameter.

To better cope with large-scale data sets, we adopt a mini-batch gradient descent optimization strategy, dividing the data set into multiple small batches, and only using a part of the samples to update the model parameters at each iteration. In a small batch gradient descent, the number of samples per small batch is set to 64. Using small batches of gradient descent can reduce computational costs, improve computational efficiency, and obtain more stability during training. To ensure the stability of the training process and improve the convergence speed, the initial learning rate is set to 0.005. By combining the Adam algorithm and small batch gradient descent, more accurate results can be obtained in model training. To prevent the problem of gradient explosion in the training process, the gradient threshold is set to 1. If the gradient of any parameter exceeds this threshold, the gradient is clipped to limit it to a controllable range. This strategy helps to maintain the stability of model training and prevent numerical problems that may be caused by gradient explosion. To improve the model's ability to generalize the data, we randomly rearrange the data before each training cycle. In this way, the model is exposed to more diverse data in each small batch of training, helping prevent overfitting and improve performance on unseen data.

The LSTM training flow chart is shown in Fig.3.

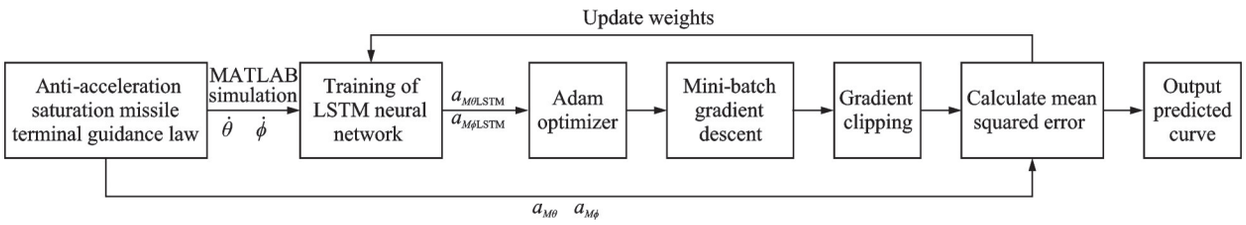

Fig.3 LSTM training flow chart

3 Simulation and Result Analysis

3.1 Simulation results

The initial condition is set as: $t_f = 10$ s, $\tau = 0.5$ s, $r_0 = 3\,000$ m, $\dot{r}_0 = 100$ m/s, $a_{M\theta\max} = a_{M\phi\max} = 100$ m/s^2, $\phi(0) = \pi/3$, $x_1(0) = 0.05$ rad/s, $x_2(0) = 0.01$ rad/s, $x_3(0) = x_4(0) = -100$ m/s^2.

Assume a weaving target maneuver with sinusoidal acceleration $a_{T\theta} = 50\sin(4\pi t)$ m/s^2, $a_{T\phi} = 50\cos(4\pi t)$ m/s^2. To demonstrate the anti-saturation characteristics of LSTM-ASGL, it is compared with the sliding mode guidance law (SMGL) proposed in Ref.[16].

The simulation results are shown in Fig.4. It can be seen that although the target can perform high-frequency sinusoidal maneuvers, the LSTM-ASGL still prevents missile acceleration saturation compared to the SMGL proposed in Ref.[16].

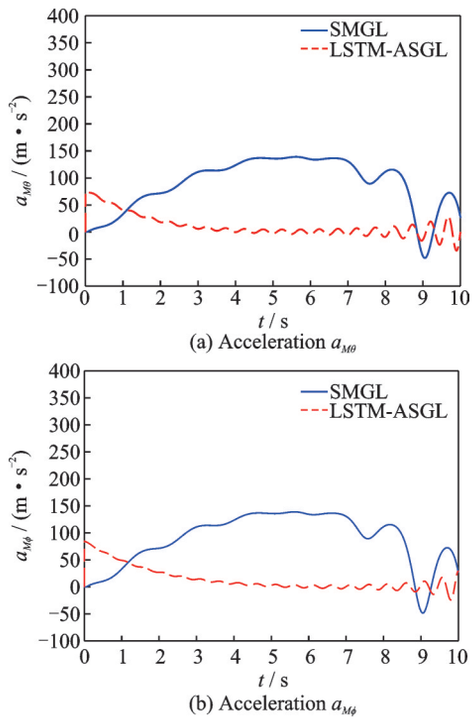

Fig.4 Acceleration comparison for a sinusoidal maneuvering target

Fig.5 shows the acceleration comparison between the anti-acceleration terminal guidance law and LSTM-ASGL. As can be seen, they match very well.

It can be seen that the acceleration curve predicted by LSTM-ASGL closely resembles the curve of the original anti-acceleration saturation guidance law, which shows the ability of the LSTM-ASGL model in capturing complex dynamics.

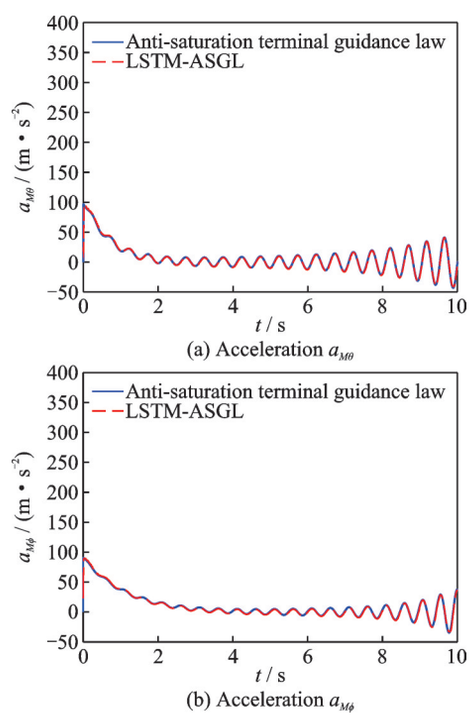

Fig.5 Acceleration comparison

The 3D trajectory diagram under sinusoidal maneuver is shown in Fig.6.

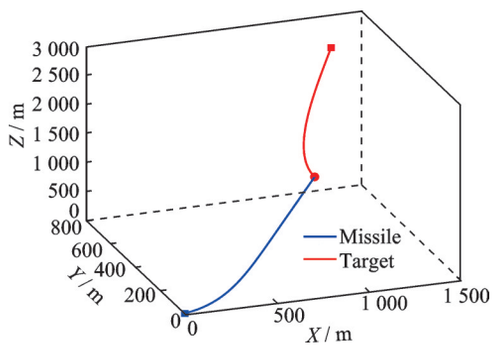

Fig.6 3D trajectory under sinusoidal maneuver

It can be seen that LSTM-ASGL can achieve the interception mission of target performing a sinusoidal maneuver.

During the prediction process, LSTM-ASGL requires only 0.52 s for computation after training, whereas the original guidance law takes 3.18 s. This significantly improves computational efficiency, demonstrating that LSTM-ASGL can greatly reduce computation time during the guidance process, making it more suitable for real-time guidance requirements.

To further verify the performance of LSTM-ASGL, the consumed energy is used to evaluate the guidance law performance. The energy consumption is given as

$$\text{Energy} = \int_0^t (a_{M\theta} + a_{M\phi})^2 \mathrm{d}t \tag{27}$$

where t is the convergence time.

Monte Carlo simulation can reliably verify the robustness of energy loss reduction advantages. Monte Carlo simulations of LSTM-ASGL under these conditions are performed 100 times, and 30% of the data are randomly selected from the training set and the test set seperately for simulation each time. The simulation results are shown in Fig.7.

The energy consumption of the original anti-acceleration saturation guidance law is 10 619.28, and the average energy consumption of the LSTM-ASGL in the 100 simulations is 10 531.70, which is

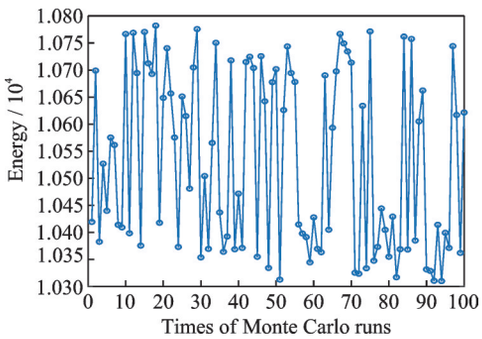

Fig.7 Monte Carlo simulation results of energy consumption for a sinusoidal maneuvering target

lower than the original anti-acceleration saturation guidance law, indicating that LSTM-ASGL can achieve target interception with lower energy.

To further verify the superiority of LSTM-ASGL, it is compared with deep neural network (DNN), convolutional neural network (CNN) and gated recurrent unit (GRU) neural networks and evaluated in terms of mean squared error (MSE) and energy consumption. The formula for MSE is given as

$$\mathrm{MSE}=\frac{1}{N}\sum_{n=1}^{N}(f_n-y_n)^2 \tag{28}$$

where f_n is the predicted value and y_n the actual value.

To further demonstrate the superiority of LSTM-ASGL in predicting anti-acceleration saturation, a comparison of training times with other neural networks is conducted. The experiment uses a sinusoidal maneuver dataset under initial conditions. The minimum error is set to 0.000 1, and the training efficiency of different networks are measured by calculating the time required for each model to reach this minimum error.

The results are shown in Table 1. As shown in Table 1, LSTM exhibits significantly lower energy consumption compared to ASGL and other neural networks. Additionally, its predicted MSE and train time are consistently lower than those of the other models. These results confirm that LSTM is the most effective neural network for handling missile acceleration saturation while also achieving the lowest energy consumption.

Table 1 Performance comparison

Model	MSE		Train time/s	Energy consumption
	$a_{M\theta}$	$a_{M\phi}$		
ASGL				10 619.28
LSTM	0.72	0.82	404	10 531.70
DNN	1.14	1.35	558	10 599.42
CNN	1.21	1.32	632	10 644.96
GRU	0.97	1.33	477	10 581.67

In missile terminal guidance, target maneuvering and acceleration saturation are time-dependent, requiring the controller to use historical information to predict target behavior and adjust strategies in advance. LSTM's gating mechanism accurately captures long-term temporal dependencies. In contrast, DNN and CNN cannot handle temporal dependencies, struggling to adapt to time-varying target maneuvers; while GRU processes temporal information, its simplified gating mechanism results in inferior performance to LSTM.

Next, a constant maneuvering target is considered with $a_{T\theta}=a_{T\phi}=50\ \mathrm{m/s^2}$. The simulation results are shown in Fig.8.

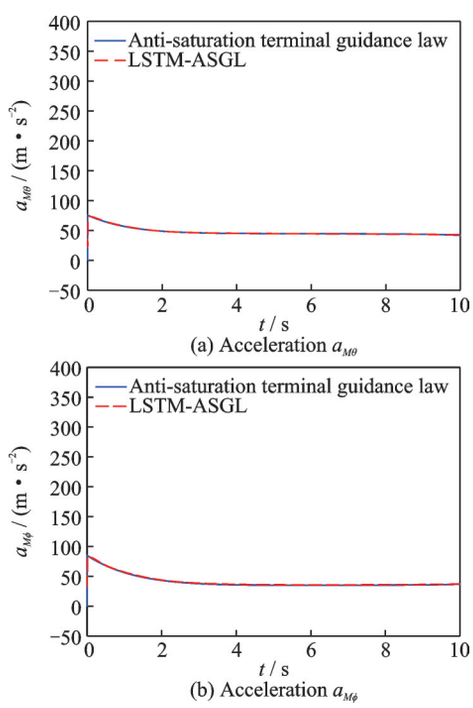

Fig.8 Acceleration comparison for a constant maneuvering target

It can be seen that under constant maneuvering of the target, the LSTM-ASGL, even without acceleration constraints, is still able to naturally counter acceleration saturation and converge effectively, achieving excellent results.

The 3D trajectory diagram under constant maneuver is shown in Fig.9. It can be seen that LSTM-

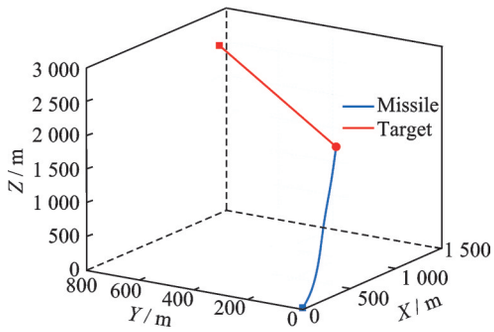

Fig.9 3D trajectory under constant maneuver

ASGL can achieve the interception mission of target performing a constant maneuver.

Similarly, 100 Monte Carlo simulations of LSTM-ASGL for this target are performed, and 30% of the data are randomly selected in the training set and the test set, respectively. The simulation results are shown in Fig.10.

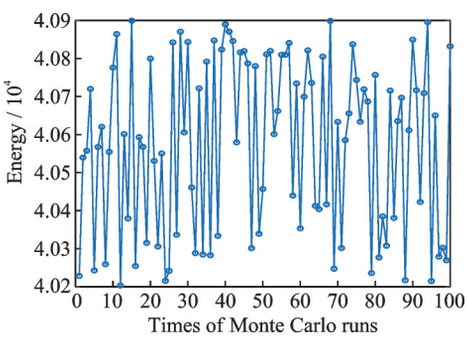

Fig.10 Monte Carlo simulation results of energy consumption for a constant maneuvering target

The energy consumption of the original anti-acceleration saturation terminal guidance law for the constant maneuvering target is 40 718.13, while the average energy consumption of LSTM-ASGL in the 100 Monte Carlo simulations is 40 576.85, which is lower than the former.

A triangular maneuvering target is considered with $a_{T\theta}=a_{T\phi}=25\text{sawtooth}(2\pi t)$ m/s^2. The simulation results are shown in Fig.11. It can be seen that under triangular maneuvering of the target, LSTM-ASGL still effectively avoids acceleration saturation and converges smoothly.

The 3D trajectory diagram under triangular maneuver is shown in Fig. 12. It can be seen that LSTM-ASGL can achieve the interception mission of target performing a triangular maneuver.

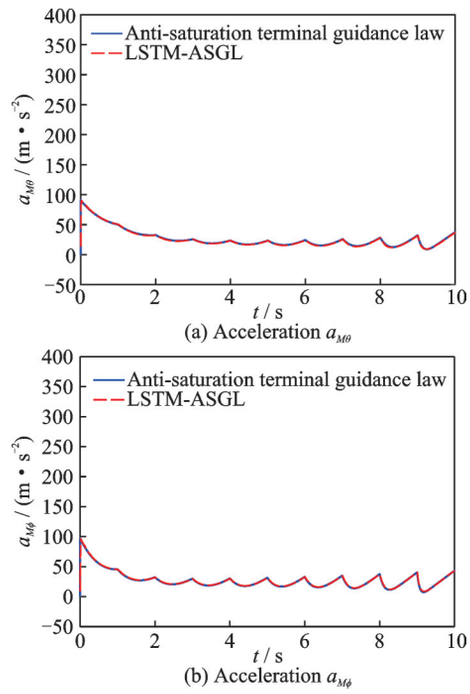

Fig.11 Acceleration comparison for a triangular maneuvering target

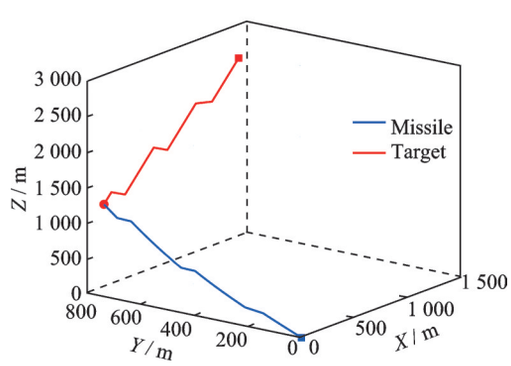

Fig.12 3D trajectory under triangular maneuver

We carry out 100 Monte Carlo simulations for the triangular maneuvering target, and 30% of the data are randomly selected in the training set and the test set separately. The simulation results are shown in Fig.13.

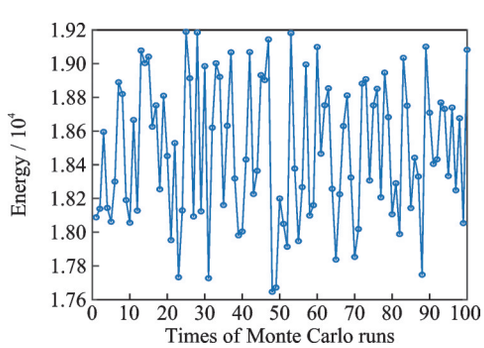

Fig.13 Monte Carlo simulation results of energy consumption for a triangular maneuvering target

The energy consumption of the original anti-acceleration saturation terminal guidance law is 18 612.85, while the average energy consumption of LSTM-ASGL in the 100 Monte Carlo simulations is 18 477.34, which is lower than the former.

From the simulation results of the three types of maneuvering targets, it can be concluded that LSTM-ASGL achieves the anti-saturation characteristics. Through the simulation study of these three types of maneuvers, it can be observed that LSTM-ASGL has an accurate acceleration prediction ability. In addition, LSTM-ASGL can achieve lower energy consumption than the original anti-acceleration saturation guidance law.

Overall, LSTM-ASGL demonstrates practical significance to improve the guidance accuracy and adaptability of the guidance system.

3.2 Generalization performance test

Two different initial conditions are set as: $\phi(0)=\pi/4$, $x_1(0)=0.06$ rad/s, $x_2(0)=0.08$ rad/s and $\phi(0)=\pi/6$, $x_1(0)=0.04$ rad/s, $x_2(0)=0.12$ rad/s. A training set is setup. The data from the initial conditions of the first experimental setup are used as the test set to verify LSTM-ASGL generalization performance for unknown data, and the predicted results are shown in Fig.14.

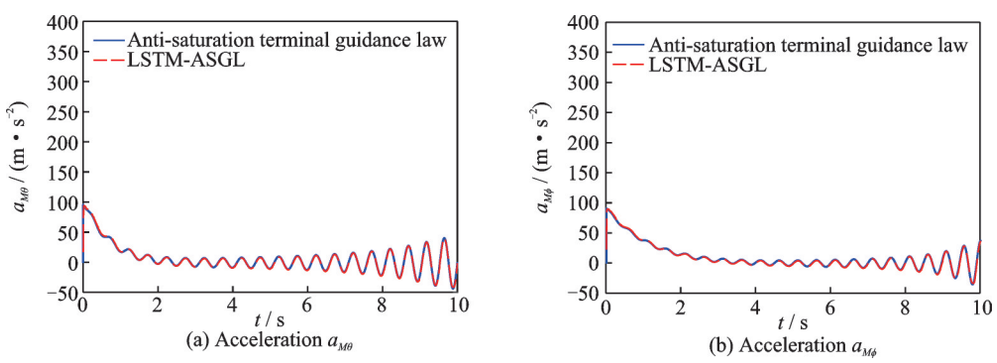

Fig.14 Acceleration curve comparison chart

3.3 Robustness test

To verify the robust performance of the neural network, a disturbance is added to the target acceleration, and the robustness is assessed. The disturbance follows a standard normal distribution (mean of 0 and standard deviation of 1) and is multiplied by a disturbance magnitude (magnitude=2) to control its size. The normal distribution effectively characterizes uncertain target motions and realistically simulates missile interference in combat. To verify the robustness of the neural network, the guidance law data set without disturbance is taken as the training set, and the guidance law data after disturbance is taken as the test set. The missile accelerations for intercepting the sinusoidal maneuvering target, the constant maneuvering target, and the triangular maneuvering target with disturbance are shown in Figs.15, 16, and 17, respectively.

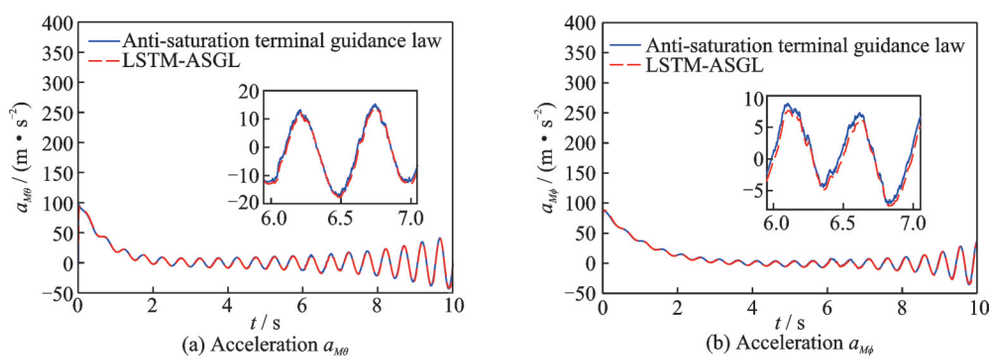

Fig.15 Acceleration comparison for a sinusoidal maneuvering target

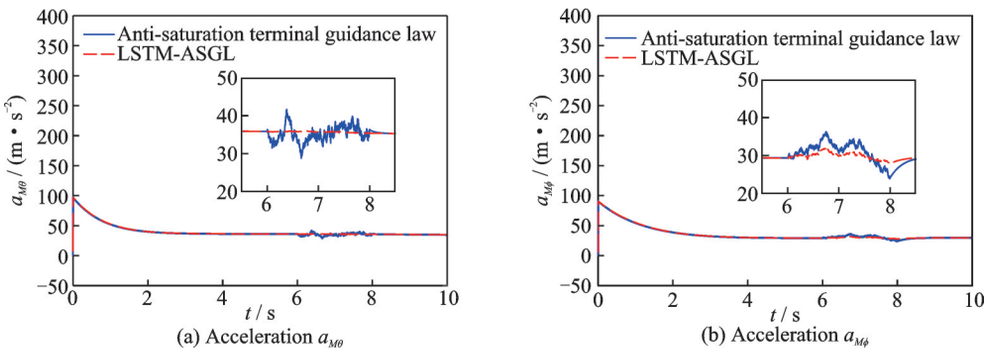

(a) Acceleration $a_{M\theta}$ (b) Acceleration $a_{M\phi}$

Fig.16 Acceleration comparison for a constant maneuvering target

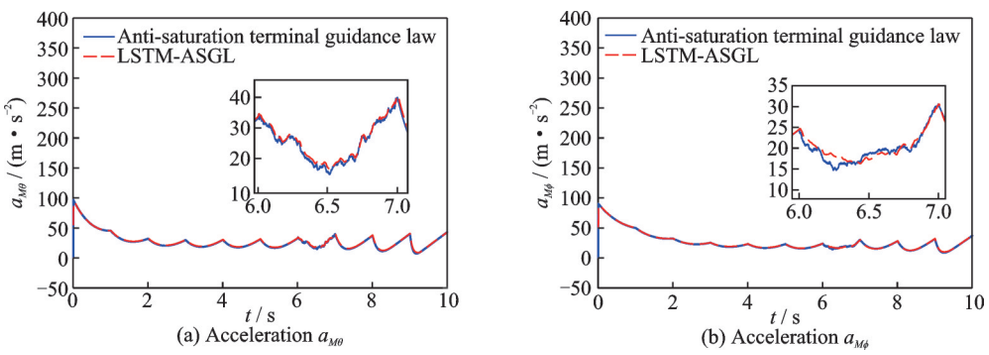

(a) Acceleration $a_{M\theta}$ (b) Acceleration $a_{M\phi}$

Fig.17 Acceleration comparison for a triangular maneuvering target

The simulation results show that the neural network has remarkable anti-jamming performance when facing different types of maneuvering targets. LSTM-ASGL successfully learns and adapts to the disturbance. Therefore, the LSTM-ASGL has a strong robustness in practical applications, and provides reliable theoretical support for its application in complex environments.

4 Conclusions

This paper studies the application of LSTM in missile terminal guidance. Aiming at the anti-acceleration saturation terminal guidance law, the designed LSTM-ASGL successfully captures and predicts the target maneuvers and has good anti-acceleration saturation characteristics. Furthermore, LSTM-ASGL demonstrates superior generalization performance on previously unknown data, demonstrating its ability to adapt to different engagement scenarios. Meanwhile, the calculation time of the LSTM-ASGL is also much lower than that of the original anti-acceleration saturation guidance law. In the robustness test, LSTM-ASGL successfully processes the disturbance data and shows good anti-jamming ability. The excellent performance of LSTM-ASGL in different maneuverability, generalization, and anti-jamming tests substantiates its broad application prospect in missile terminal guidance systems.

References

[1] LI G L, XIN M. A three-dimensional anti-saturation terminal guidance law with finite-time convergence[C]//Proceedings of 2017 American Control Conference. Seattle, USA: IEEE, 2017: 2243-2248.

[2] YU J, LEI J, WANG H, et al. Research on an extended composite proportional navigation law based on error adaptation and error anti saturation[J]. Journal of Electronics and Information Science, 2022, 7(4): 1-8.

[3] DONG W, WANG C Y, WANG J N, et al. Varying-gain proportional navigation guidance for precise impact time control[J]. Journal of Guidance, Control, and Dynamics, 2022, 46(3): 535-552.

[4] MA M C, TAN L G, SONG S M. Three-dimensional sliding mode guidance law for maneuvering target with prescribed performance and input saturation[J]. Transactions of the Institute of Measurement and Control, 2021, 43(5): 1176-1190.

[5] WU G, ZHANG K. A novel fixed-time convergence three-dimensional guidance law for intercepting highly maneuvering targets[J]. International Journal of Aeronautical and Space Sciences, 2022, 23(3): 595-608.

[6] SI Y J, SONG S M. Adaptive reaching law based three-dimensional finite-time guidance law against maneuvering targets with input saturation[J]. Aerospace Science and Technology, 2017, 70: 198-210.

[7] WANG X X, LAN G, YANG Y F, et al. Terminal angle constrained time-varying sliding mode guidance law with autopilot dynamics and input saturation[J]. Asian Journal of Control, 2023, 25(2): 1130-1144.
[8] KIM M, HONG D, PARK S. Deep neural network-based guidance law using supervised learning[J]. Applied Sciences, 2020, 10(21): 7865.
[9] YANG Z Q, LIU X D, LIU H K. Impact time control guidance law with time-varying velocity based on deep reinforcement learning[J]. Aerospace Science and Technology, 2023, 142: 108603.
[10] CHENG L, WANG H, GONG S P, et al. Neural-network-based nonlinear optimal terminal guidance with impact angle constraints[J]. IEEE Transactions on Aerospace and Electronic Systems, 2024, 60(1): 819-830.
[11] LI Z, WU J Z, WU Y P, et al. Real-time guidance strategy for active defense aircraft via deep reinforcement learning[C]//Proceedings of NAECON 2021-IEEE National Aerospace and Electronics Conference. Dayton, USA: IEEE, 2021: 177-183.
[12] JIN T Y, HE S M. Ensemble transfer learning midcourse guidance algorithm for velocity maximization[J]. Journal of Aerospace Information Systems, 2023, 20(4): 204-215.
[13] HU Z, XIAO L, GUAN J, et al. Intercept guidance of maneuvering targets with deep reinforcement learning[J]. International Journal of Aerospace Engineering, 2023, 2023: 7924190.
[14] QIU X Q, LAI P, GAO C S, et al. Recorded recurrent deep reinforcement learning guidance laws for intercepting endoatmospheric maneuvering missiles[J]. Defence Technology, 2024, 31: 457-470.
[15] SONG J, XU X W, TONG X D, et al. A time cooperation guidance for multi-hypersonic vehicles based on LSTM network and improved artificial potential field method[J]. Aerospace, 2022, 9(10): 562.
[16] DONG F, ZHANG X Y, TAN P L. Non-singular terminal sliding mode cooperative guidance law under impact angle constraint[J]. Journal of the Franklin Institute, 2024, 361(14): 107079.

Authors

The first author Dr. **LI Guilin** received her B.E. degree in industrial automation from China University of Mining and Technology in 1998 and Ph.D. degree in control science and engineering from University of Science and Technology of China in 2015. She joined School of Electrical Engineering and Automation, Jiangsu Normal University in 2005, where she is an associate professor. Her research is focused on missile guidance law and deep learning.

The corresponding author Mr. **ZHOU Wei** received his B.E. degree in automation from Anhui University of Science and Technology in 2022, and M.E. degree in electronic information engineering from Jiangsu Normal University in 2025. His research is focused on missile guidance and deep learning.

Author contributions Dr. **LI Guilin** contributed to the development of the original anti-acceleration saturation terminal guidance law that is the main subject of this manuscript. She also provided the main technical advice on the revision of the manuscript and the response letter to address the reviewers' comments. Mr. **ZHOU Wei** prepared the model, designed the experiment, analyzed the results, and wrote the manuscript. Dr. **ZHANG Jiarui** made a significant contribution to the English writing. All authors commented on the manuscript draft and approved the submission.

Competing interests The authors declare no competing interests.

(Prodution Editor: ZHANG Bei)

基于LSTM的抗加速度饱和导弹末制导律

李桂林，周　围，张嘉睿

(江苏师范大学电气工程及自动化学院，徐州 221116，中国)

摘要：在实际末制导过程中，导弹加速度饱和可能显著降低拦截性能。针对这一问题，本文提出一种适用于三维机动拦截的有限时间收敛抗饱和制导律。该方法结合有限时间有界(Finite time boundedness, FTB)理论、输入输出有限时间稳定(Input-output finite time stability, IO-FTS)理论以及长短期记忆网络(Long short-term memory network, LSTM)，首先给出一类非线性系统的FTB和IO-FTS充分条件，然后设计了基于LSTM的抗加速度饱和导弹末制导律，称为LSLTM-ASGL。该制导律可有效抑制加速度饱和效应，在复杂动态环境中更精准地跟踪机动目标。仿真实验验证了LSTM-ASGL在不同机动目标场景下的优良性能。结果表明，该制导律成功避免了加速度饱和，提升了导弹系统对机动目标的跟踪能力，同时展现出良好的泛化性与抗干扰性能，且能量损耗低于传统抗加速度饱和末制导律。

关键词：长短期记忆网络；抗加速度饱和；末制导律；有限时间有界；输入输出有限时间稳定